

Chapter 5

Effects of Compressibility

For flows in which compressibility effects are important, we must introduce an equation for conservation of energy and an equation of state. Just as Reynolds averaging gives rise to the Reynolds-stress tensor, so we expect that similar averaging will lead to a turbulent heat-flux vector. We should also expect that new compressibility related correlations will appear throughout the equations of motion. These are important issues that must be addressed in constructing a turbulence model suitable for application to compressible flows. This chapter focuses upon these issues.

We begin with a brief discussion of common observations pertaining to compressible turbulence. Then, we introduce the Favre mass-averaging procedure and derive the mass-averaged equations of motion. Next, we demonstrate an elegant development in turbulence modeling for the compressible mixing layer. We follow this analysis with an application of perturbation methods to the compressible log layer. We then apply several models to attached compressible boundary layers, including effects of pressure gradient, surface cooling and surface roughness. The chapter concludes with application of various turbulence models to shock-separated flows.

5.1 Physical Considerations

By definition, a compressible flow is one in which significant density changes occur, even when pressure changes are small. Generally speaking, compressibility has a relatively small effect on turbulent eddies in wall-bounded flows. This appears to be true for Mach numbers up to about 5 (and perhaps as high as 8), provided the flow doesn't experience large pressure changes over a short distance such as we might have across a shock wave. At subsonic

speeds, compressibility effects on eddies are usually unimportant for boundary layers provided $T_w/T_e < 6$. Based on these observations, Morkovin (1962) hypothesized that the effect of density fluctuations on the turbulence are small provided they remain small relative to the mean density. This is a major simplification for the turbulence modeler because it means that, in practice, he need only account for the nonuniform mean density in computing compressible, shock-free, non-hypersonic turbulent flows.

There are limitations to the applicability of **Morkovin's hypothesis** even at non-hypersonic Mach numbers. For example, because $\rho'/\bar{\rho}$ is typically not small, it applies neither to flows with significant heat transfer nor to flows with combustion. Also, because density fluctuations generally are much larger in free shear flows, models based on Morkovin's hypothesis fail to predict the measured reduction in spreading rate with increasing freestream Mach number for the compressible mixing layer [Papamoschou and Roshko (1988)]. As we will see in Section 5.5, the level of $\rho'/\bar{\rho}$ for a boundary layer at Mach 5 is comparable to the level found in a mixing layer at Mach 1. For Mach numbers in excess of 1, the spreading rate for a mixing layer decreases. This is consistent with Mach 5 representing the hypersonic limit for the boundary layer.

As a final observation, note that the difficulty in predicting properties of the compressible mixing layer is reminiscent of our experience with free shear flows in Chapters 3 and 4. That is, we find again that the seemingly simple free shear flow case is more difficult to model than the wall-bounded case.

5.2 Favre Averaging

In addition to velocity and pressure fluctuations, we must also account for density and temperature fluctuations when the medium is a compressible fluid. If we use the standard time-averaging procedure introduced in Chapter 2, the mean conservation equations contain additional terms that have no analogs in the laminar equations. To illustrate this, consider conservation of mass. We write the instantaneous density ρ as the sum of mean, $\bar{\rho}$, and fluctuating, ρ' , parts, i.e.,

$$\rho = \bar{\rho} + \rho' \quad (5.1)$$

Expressing the instantaneous velocity in the usual way [Equation (2.4)], substituting into the continuity equation yields

$$\frac{\partial}{\partial t}(\bar{\rho} + \rho') + \frac{\partial}{\partial x_i}(\bar{\rho}U_i + \rho'U_i + \bar{\rho}u'_i + \rho'u'_i) = 0 \quad (5.2)$$

After time averaging Equation (5.2), we arrive at the Reynolds-averaged continuity equation for compressible flow, viz.,

$$\frac{\partial \bar{\rho}}{\partial t} + \frac{\partial}{\partial x_i} \left(\bar{\rho} U_i + \overline{\rho' u'_i} \right) = 0 \quad (5.3)$$

Some authors refer to this as the **primitive-variable form** of the continuity equation. Note that in order to achieve closure, an approximation for the correlation between ρ' and u'_i is needed. The problem is even more complicated for the momentum equation where the Reynolds-stress tensor originates from time averaging the product $\rho u_i u_j$ that appears in the convective acceleration. Clearly, a triple correlation involving ρ' , u'_i , and u'_j appears, thus increasing the complexity of establishing suitable closure approximations. The problem of establishing the appropriate form of the time-averaged equations can be simplified dramatically by using the density-weighted averaging procedure suggested by Favre (1965). That is, we introduce the **mass-averaged velocity**, \tilde{u}_i , defined by

$$\tilde{u}_i = \frac{1}{\bar{\rho}} \lim_{T \rightarrow \infty} \int_t^{t+T} \rho(\mathbf{x}, \tau) u_i(\mathbf{x}, \tau) d\tau \quad (5.4)$$

where $\bar{\rho}$ is the conventional Reynolds-averaged density. Thus, in terms of conventional Reynolds averaging, we can say that

$$\bar{\rho} \tilde{u}_i = \overline{\rho u_i} \quad (5.5)$$

where an overbar denotes conventional Reynolds average. The value of this averaging process, known as **Favre averaging**, becomes obvious when we expand the right-hand side of Equation (5.5). Performing the indicated Reynolds-averaging process, there follows

$$\bar{\rho} \tilde{u}_i = \bar{\rho} U_i + \overline{\rho' u'_i} \quad (5.6)$$

Inspection of Equation (5.3) shows that conservation of mass can be rewritten as

$$\frac{\partial \bar{\rho}}{\partial t} + \frac{\partial}{\partial x_i} (\bar{\rho} \tilde{u}_i) = 0 \quad (5.7)$$

This is a remarkable simplification as Equation (5.7) looks just like the laminar mass-conservation equation. What we have done is treat the momentum per unit volume, ρu_i , as the dependent variable rather than the velocity. This is a sensible thing to do from a physical point of view, especially when we focus upon the momentum equation in the next section. That is, the rate of change of momentum per unit volume, not velocity, is equal to the sum of the imposed forces per unit volume in a flow.

When we use Favre averaging, it is customary to decompose the instantaneous velocity into the mass-averaged part, \tilde{u}_i , and a fluctuating part, u_i'' , wherefore

$$u_i = \tilde{u}_i + u_i'' \quad (5.8)$$

Now, to form the Favre average, we simply multiply through by ρ and do a time average in the manner established in Chapter 2. Hence, from Equation (5.8) we find

$$\overline{\rho u_i} = \bar{\rho} \tilde{u}_i + \overline{\rho u_i''} \quad (5.9)$$

But, from the definition of the Favre average given in Equation (5.5), we see immediately that, as expected, the Favre average of the fluctuating velocity, u_i'' , vanishes, i.e.,

$$\overline{\rho u_i''} = 0 \quad (5.10)$$

By contrast, the conventional Reynolds average of u_i'' is not zero. To see this, note that

$$u_i'' = u_i - \tilde{u}_i \quad (5.11)$$

Hence, using Equation (5.6) to eliminate \tilde{u}_i ,

$$u_i'' = u_i - U_i - \frac{\overline{\rho' u_i'}}{\bar{\rho}} \quad (5.12)$$

Therefore, performing the conventional Reynolds average, we find

$$\overline{u_i''} = -\frac{\overline{\rho' u_i'}}{\bar{\rho}} \neq 0 \quad (5.13)$$

As a final comment, do not lose sight of the fact that while Favre averaging eliminates density fluctuations from the averaged equations, it does not remove the effect the density fluctuations have on the turbulence. Consequently, **Favre averaging is a mathematical simplification, not a physical one.**

5.3 Favre-Averaged Equations

For motion in a compressible medium, we must solve the equations governing conservation of mass, momentum and energy. The instantaneous equations are as follows:

$$\frac{\partial \rho}{\partial t} + \frac{\partial}{\partial x_i}(\rho u_i) = 0 \quad (5.14)$$

$$\frac{\partial}{\partial t}(\rho u_i) + \frac{\partial}{\partial x_j}(\rho u_j u_i) = -\frac{\partial p}{\partial x_i} + \frac{\partial t_{ji}}{\partial x_j} \quad (5.15)$$

$$\frac{\partial}{\partial t} \left[\rho \left(e + \frac{1}{2} u_i u_i \right) \right] + \frac{\partial}{\partial x_j} \left[\rho u_j \left(h + \frac{1}{2} u_i u_i \right) \right] = \frac{\partial}{\partial x_j} (u_i t_{ij}) - \frac{\partial q_j}{\partial x_j} \quad (5.16)$$

where e is specific internal energy and $h = e + p/\rho$ is specific enthalpy. For compressible flow, the viscous stress tensor, t_{ij} , involves the second viscosity, ζ , as well as the conventional molecular viscosity, μ . Although it is not necessary for our immediate purposes, we eventually must specify an equation of state. For gases, we use the perfect gas law so that pressure, density and temperature are related by

$$p = \rho RT \quad (5.17)$$

where R is the perfect gas constant. The constitutive relation between stress and strain rate for a Newtonian fluid is

$$t_{ij} = 2\mu s_{ij} + \zeta \frac{\partial u_k}{\partial x_k} \delta_{ij} \quad (5.18)$$

where s_{ij} is the instantaneous strain-rate tensor [Equation (2.19)] and δ_{ij} is the Kronecker delta. The heat-flux vector, q_j , is usually obtained from Fourier's law so that

$$q_j = -\kappa \frac{\partial T}{\partial x_j} \quad (5.19)$$

where κ is thermal conductivity. We can simplify our analysis somewhat by introducing two commonly used assumptions. First, we relate second viscosity to μ by assuming

$$\zeta = -\frac{2}{3}\mu \quad (5.20)$$

This assumption is correct for a monatomic gas, and is generally used for all gases in standard CFD applications. Assuming Equation (5.20) holds in general guarantees $t_{ii} = 0$ so that viscous stresses do not contribute to the pressure, even when $s_{ii} = \partial u_i / \partial x_i \neq 0$. This is tidy, even if not necessarily true. Second, we assume the fluid is calorically perfect so that its specific heat coefficients are constant, and thus

$$e = C_v T \quad \text{and} \quad h = C_p T \quad (5.21)$$

where C_v and C_p are the specific heat coefficients for constant volume and pressure processes, respectively. Then, we can say that

$$q_j = -\kappa \frac{\partial T}{\partial x_j} = -\frac{\mu}{Pr_L} \frac{\partial h}{\partial x_j} \quad (5.22)$$

where Pr_L is the **laminar Prandtl number** defined by

$$Pr_L = \frac{C_p \mu}{\kappa} \quad (5.23)$$

In order to mass average the conservation equations, we now decompose the various flow properties as follows.

$$\left. \begin{aligned} u_i &= \tilde{u}_i + u_i'' \\ \rho &= \bar{\rho} + \rho' \\ p &= P + p' \\ h &= \tilde{h} + h'' \\ e &= \tilde{e} + e'' \\ T &= \tilde{T} + T'' \\ q_j &= q_{Lj} + q_j' \end{aligned} \right\} \quad (5.24)$$

Note that we decompose p , ρ and q_j in terms of conventional mean and fluctuating parts. Substituting Equations (5.24) into Equations (5.14) - (5.17) and performing the mass-averaging operations, we arrive at what are generally referred to as the **Favre (mass) averaged mean conservation equations**.

$$\frac{\partial \bar{\rho}}{\partial t} + \frac{\partial}{\partial x_i} (\bar{\rho} \tilde{u}_i) = 0 \quad (5.25)$$

$$\frac{\partial}{\partial t} (\bar{\rho} \tilde{u}_i) + \frac{\partial}{\partial x_j} (\bar{\rho} \tilde{u}_j \tilde{u}_i) = - \frac{\partial P}{\partial x_i} + \frac{\partial}{\partial x_j} [\bar{t}_{ji} - \overline{\rho u_j'' u_i''}] \quad (5.26)$$

$$\begin{aligned} \frac{\partial}{\partial t} \left[\bar{\rho} \left(\tilde{e} + \frac{\tilde{u}_i \tilde{u}_i}{2} \right) + \frac{\overline{\rho u_i'' u_i''}}{2} \right] + \frac{\partial}{\partial x_j} \left[\bar{\rho} \tilde{u}_j \left(\tilde{h} + \frac{\tilde{u}_i \tilde{u}_i}{2} \right) + \tilde{u}_j \frac{\overline{\rho u_i'' u_i''}}{2} \right] \\ = \frac{\partial}{\partial x_j} \left[-q_{Lj} - \overline{\rho u_j'' h''} + \bar{t}_{ji} u_i'' - \overline{\rho u_j'' \frac{1}{2} u_i'' u_i''} \right] \\ + \frac{\partial}{\partial x_j} \left[\tilde{u}_i \left(\bar{t}_{ij} - \overline{\rho u_i'' u_j''} \right) \right] \quad (5.27) \end{aligned}$$

$$P = \bar{\rho} R \tilde{T} \quad (5.28)$$

Equations (5.25), (5.26) and (5.28) differ from their laminar counterparts only by the appearance of the Favre-averaged Reynolds-stress tensor, viz.,

$$\tau_{ij} = -\overline{\rho u_i'' u_j''} \quad (5.29)$$

As in the incompressible case, the Favre-averaged τ_{ij} is a symmetric tensor.

The Favre-averaged mean energy equation for total energy, i.e., the sum of internal energy, mean-flow kinetic energy and turbulence kinetic energy has numerous additional terms, each of which represents an identifiable physical process or property. Consider first the double correlation between

u_i'' and itself that appears in each of the two terms on the left-hand side of Equation (5.27). This is the kinetic energy per unit volume of the turbulent fluctuations, so that it makes sense to define

$$\bar{\rho}k = \frac{1}{2} \overline{\rho u_i'' u_i''} \quad (5.30)$$

Next, the correlation between u_j'' and h'' is the turbulent transport of heat. In analogy to the notation selected for the molecular transport of heat, we define

$$qT_j = \overline{\rho u_j'' h''} \quad (5.31)$$

The two terms $\overline{t_{ji} u_i''}$ and $\overline{\rho u_j'' \frac{1}{2} u_i'' u_i''}$ on the right-hand side of Equation (5.27) correspond to molecular diffusion and turbulent transport of turbulence kinetic energy, respectively. These terms arise because the mass-averaged total enthalpy appearing in the convective term of Equation (5.27) is the sum of mass-averaged enthalpy, mean kinetic energy and turbulence kinetic energy. They represent transfers between mean energy and turbulence kinetic energy, that naturally arise when we derive the Favre-averaged turbulence kinetic energy equation. The simplest way to derive the equation for k is to multiply the primitive-variable form of the instantaneous momentum equation by u_i'' and time average.

$$\overline{\rho u_i'' \frac{\partial u_i}{\partial t}} + \overline{\rho u_i'' u_j \frac{\partial u_i}{\partial x_j}} = -\overline{u_i'' \frac{\partial p}{\partial x_i}} + \overline{u_i'' \frac{\partial t_{ji}}{\partial x_j}} \quad (5.32)$$

As in Chapter 2, the most illuminating way to carry out the indicated time-averaging operations is to proceed term by term, and to use tensor notation for all derivatives. Proceeding from left to right, we first consider the **unsteady term**.

$$\begin{aligned} \overline{\rho u_i'' u_{i,t}} &= \overline{\rho u_i'' (\tilde{u}_i + u_i'')_{,t}} \\ &= \overline{\rho u_i'' \tilde{u}_{i,t}} + \overline{\rho u_i'' u_{i,t}''} \\ &= \overline{\rho (\frac{1}{2} u_i'' u_i'')_{,t}} \\ &= \frac{\partial}{\partial t} (\bar{\rho}k) - \frac{1}{2} \overline{u_i'' u_i'' \frac{\partial \rho}{\partial t}} \end{aligned} \quad (5.33)$$

Turning now to the **convective term**, we have the following.

$$\begin{aligned}
 \overline{\rho u_i'' u_j u_{i,j}} &= \overline{\rho u_i'' [(\tilde{u}_j + u_j'') \tilde{u}_{i,j} + u_j u_{i,j}'']} \\
 &= \overline{\rho u_i'' \tilde{u}_j \tilde{u}_{i,j}} + \overline{\rho u_i'' u_j' \tilde{u}_{i,j}} + \overline{\rho u_j u_i'' u_{i,j}''} \\
 &= -\tau_{ij} \tilde{u}_{i,j} + \overline{\rho u_j (\frac{1}{2} u_i'' u_i'')_{,j}} \\
 &= -\tau_{ij} \tilde{u}_{i,j} + \overline{(\rho u_j \frac{1}{2} u_i'' u_i'')_{,j}} - \frac{1}{2} \overline{u_i'' u_i'' (\rho u_j)_{,j}} \\
 &= -\tau_{ij} \tilde{u}_{i,j} + \left(\overline{\rho \tilde{u}_j \frac{1}{2} u_i'' u_i''} + \overline{\rho u_j' \frac{1}{2} u_i'' u_i''} \right)_{,j} - \frac{1}{2} \overline{u_i'' u_i'' (\rho u_j)_{,j}} \\
 &= -\tau_{ij} \frac{\partial \tilde{u}_i}{\partial x_j} + \frac{\partial}{\partial x_j} \left(\overline{\rho \tilde{u}_j k} + \overline{\rho u_j' \frac{1}{2} u_i'' u_i''} \right) - \frac{1}{2} \overline{u_i'' u_i''} \frac{\partial}{\partial x_j} (\rho u_j)
 \end{aligned} \tag{5.34}$$

The **pressure gradient term** simplifies immediately as follows.

$$\overline{u_i'' p_{,i}} = \overline{u_i'' P_{,i}} + \overline{u_i'' p'_{,i}} = \overline{u_i''} \frac{\partial P}{\partial x_i} + \frac{\partial}{\partial x_i} \left(\overline{p' u_i''} \right) - p' \frac{\partial \overline{u_i''}}{\partial x_i} \tag{5.35}$$

Finally, the **viscous term** is simply rewritten as

$$\overline{u_i'' t_{j,i,j}} = \frac{\partial}{\partial x_j} \left(\overline{t_{j,i} u_i''} \right) - \overline{t_{j,i}} \frac{\partial \overline{u_i''}}{\partial x_j} \tag{5.36}$$

Thus, substituting Equations (5.33) through (5.36) into Equation (5.32), we arrive at the **Favre-averaged turbulence kinetic energy equation**. In arriving at the final result, we make use of the fact that the sum of the last terms on the right-hand sides of Equations (5.33) and (5.34) vanish since their sum is proportional to the two terms appearing in the instantaneous continuity equation. Additionally, to facilitate comparison with the incompressible turbulence kinetic energy equation [Equation (4.4)], we use the Favre-averaged continuity equation to rewrite the unsteady and convective terms in non-conservation form. The exact equation is as follows.

$$\begin{aligned}
 \bar{\rho} \frac{\partial k}{\partial t} + \bar{\rho} \tilde{u}_j \frac{\partial k}{\partial x_j} &= \tau_{ij} \frac{\partial \tilde{u}_i}{\partial x_j} - \overline{t_{j,i}} \frac{\partial \overline{u_i''}}{\partial x_j} + \frac{\partial}{\partial x_j} \left[\overline{t_{j,i} u_i''} - \overline{\rho u_j' \frac{1}{2} u_i'' u_i''} - \overline{p' u_i''} \right] \\
 &\quad - \underbrace{\overline{u_i''} \frac{\partial P}{\partial x_i}}_{\text{Pressure Work}} + \underbrace{\overline{p' \frac{\partial u_i''}{\partial x_i}}}_{\text{Pressure Dilatation}}
 \end{aligned} \tag{5.37}$$

Comparing the mean energy Equation (5.27) with the turbulence kinetic energy Equation (5.37), we see that indeed the two terms $\overline{t_{j,i} u_i''}$ and

$\overline{\rho u_j'' \frac{1}{2} u_i'' u_i''}$ on the right-hand side of the mean-energy equation are **Molecular Diffusion** and **Turbulent Transport** of turbulence kinetic energy. Inspection of the turbulence kinetic energy equation also indicates that the **Favre-averaged dissipation rate** is given by

$$\bar{\rho}\epsilon = t_{ji} \overline{\frac{\partial u_i''}{\partial x_j}} \quad (5.38)$$

Comparison of Equation (5.37) with the incompressible equation for k [Equation (4.4)] shows that all except the last two terms, i.e., the **Pressure Work** and **Pressure-Dilatation** terms, have analogs in the incompressible equation. Both of these terms vanish in the limit of incompressible flow with zero density fluctuations. The **Pressure Work** vanishes because the time average of u_i'' is zero when density fluctuations are zero. The **Pressure-Dilatation** term vanishes because the fluctuating field has zero divergence for incompressible flow. Hence, Equation (5.37) simplifies to Equation (4.4) for incompressible flow with zero density fluctuations.

Note that the turbulence kinetic energy production, $\tau_{ij} \partial \tilde{u}_i / \partial x_j$, and pressure correlation terms represent a transfer from mean kinetic energy to turbulence kinetic energy. Also, dissipation is a transfer from turbulence kinetic energy to internal energy. Thus, since these transfers simply redistribute energy, they must cancel in the overall energy conservation equation. Consequently, only the two terms involving spatial transport of turbulence kinetic energy appear in Equation (5.27).

Using a similar derivation (we omit the details here for the sake of brevity), the **Favre-averaged Reynolds-stress equation** assumes the following form.

$$\begin{aligned} \frac{\partial \tau_{ij}}{\partial t} + \frac{\partial}{\partial x_k} (\tilde{u}_k \tau_{ij}) &= -\tau_{ik} \frac{\partial \tilde{u}_j}{\partial x_k} - \tau_{jk} \frac{\partial \tilde{u}_i}{\partial x_k} + \epsilon_{ij} - \Pi_{ij} \\ &+ \frac{\partial}{\partial x_k} \left[-\overline{(t_{kj} u_i'' + t_{ki} u_j'')} + C_{ijk} \right] \\ &+ \overline{u_i''} \frac{\partial P}{\partial x_j} + \overline{u_j''} \frac{\partial P}{\partial x_i} \end{aligned} \quad (5.39)$$

where

$$\Pi_{ij} = p' \left(\frac{\partial u_i''}{\partial x_j} + \frac{\partial u_j''}{\partial x_i} \right) \quad (5.40)$$

$$\epsilon_{ij} = t_{kj} \overline{\frac{\partial u_i''}{\partial x_k}} + t_{ki} \overline{\frac{\partial u_j''}{\partial x_k}} \quad (5.41)$$

$$C_{ijk} = \overline{\rho u_i'' u_j'' u_k''} + \overline{p' u_i''} \delta_{jk} + \overline{p' u_j''} \delta_{ik} \quad (5.42)$$

Taking advantage of the definitions given in Equations (5.29), (5.30), (5.31) and (5.38), we can summarize the Favre-averaged mean equations and turbulence kinetic energy equation in conservation form.

$$\frac{\partial \bar{\rho}}{\partial t} + \frac{\partial}{\partial x_i} (\bar{\rho} \tilde{u}_i) = 0 \quad (5.43)$$

$$\frac{\partial}{\partial t} (\bar{\rho} \tilde{u}_i) + \frac{\partial}{\partial x_j} (\bar{\rho} \tilde{u}_j \tilde{u}_i) = -\frac{\partial P}{\partial x_i} + \frac{\partial}{\partial x_j} [\bar{t}_{ji} + \tau_{ji}] \quad (5.44)$$

$$\begin{aligned} \frac{\partial}{\partial t} (\bar{\rho} E) + \frac{\partial}{\partial x_j} (\bar{\rho} \tilde{u}_j H) &= \frac{\partial}{\partial x_j} \left[-q_{Lj} - q_{Tj} + \overline{t_{ji} u_i''} - \overline{\rho u_j'' \frac{1}{2} u_i'' u_i''} \right] \\ &+ \frac{\partial}{\partial x_j} [\tilde{u}_i (\bar{t}_{ij} + \tau_{ij})] \end{aligned} \quad (5.45)$$

$$\begin{aligned} \frac{\partial}{\partial t} (\bar{\rho} k) + \frac{\partial}{\partial x_j} (\bar{\rho} \tilde{u}_j k) &= \tau_{ij} \frac{\partial \tilde{u}_i}{\partial x_j} - \bar{\rho} \epsilon + \frac{\partial}{\partial x_j} \left[\overline{t_{ji} u_i''} - \overline{\rho u_j'' \frac{1}{2} u_i'' u_i''} - \overline{p' u_j''} \right] \\ &- \overline{u_i''} \frac{\partial P}{\partial x_i} + \overline{p' \frac{\partial u_i''}{\partial x_i}} \end{aligned} \quad (5.46)$$

$$P = \bar{\rho} R \tilde{T} \quad (5.47)$$

The quantities E and H are the **total energy** and **total enthalpy**, and include the kinetic energy of the fluctuating turbulent field, viz.,

$$E = \bar{e} + \frac{1}{2} \tilde{u}_i \tilde{u}_i + k \quad \text{and} \quad H = \bar{h} + \frac{1}{2} \tilde{u}_i \tilde{u}_i + k \quad (5.48)$$

5.4 Compressible-Flow Closure Approximations

As discussed in the preceding section, in addition to having variable mean density $\bar{\rho}$, Equations (5.39) through (5.48) reflect effects of compressibility through various correlations that are affected by fluctuating density. For all but second-order closure models, closure approximations must be postulated for the mass-averaged Reynolds-stress tensor and heat-flux vector. Depending on the type of turbulence model used, additional closure approximations may be needed to close the system of equations defining the model.

This section briefly reviews some of the most commonly used closure approximations for compressible flows. Because of the paucity of measurements compared to the incompressible case, and the additional complexities attending compressible flows, far less is available to guide development of closure approximations suitable for a wide range of applications. As a result, modeling of compressibility effects is in a continuing state of flux as we approach the end of the twentieth century. The closure approximations discussed in this, and following, sections are those that have stood the test of time.

Before focusing upon specific closure approximations, it is worthwhile to cite important guidelines that should be followed in devising compressible-flow closure approximations. Adhering to the following items will lead to the simplest and most elegant models.

1. All closure approximations should approach the proper limiting value for Mach number and density fluctuations tending to zero.
2. All closure terms should be written in proper tensor form, e.g., not dependent upon a specific geometrical configuration.
3. All closure approximations should be dimensionally consistent and invariant under a Galilean transformation.

It should be obvious that Items 2 and 3 apply for incompressible flows as well. In practice, Galilean invariance seems to be ignored more often than any other item listed, especially for compressible flows. Such models should be rejected as they violate a fundamental feature of the Navier-Stokes equation, and are thus physically unsound.

Reynolds-stress Tensor: For zero-, one- and two-equation models, nearly all researchers use the Boussinesq approximation with suitable generalization for compressible flows. Specifically, denoting the eddy viscosity by μ_T , the following form is generally assumed.

$$\tau_{ij} \equiv -\overline{\rho u_i' u_j'} = 2\mu_T \left(S_{ij} - \frac{1}{3} \frac{\partial \tilde{u}_k}{\partial x_k} \delta_{ij} \right) - \frac{2}{3} \bar{\rho} k \delta_{ij} \quad (5.49)$$

The most important consideration in postulating Equation (5.49) is guaranteeing that the trace of τ_{ij} is $-2\bar{\rho}k$. Note that this means the "second eddy viscosity" must be $-\frac{2}{3}\mu_T$ [recall Equation (5.20)].

Turbulent Heat-Flux Vector: The most commonly used closure approximation for the turbulent heat-flux vector, q_T , follows from appealing to the classical analogy [Reynolds (1874)] between momentum and heat

transfer. It is thus assumed to be proportional to the mean temperature gradient, so that

$$q_{Tj} = \overline{\rho u_j'' h''} = -\frac{\mu_T C_p}{Pr_T} \frac{\partial \tilde{T}}{\partial x_j} = -\frac{\mu_T}{Pr_T} \frac{\partial \tilde{h}}{\partial x_j} \quad (5.50)$$

where Pr_T is the **turbulent Prandtl number**. A constant value for Pr_T is often used and this is usually satisfactory for shock-free flows up to low supersonic speeds, provided the heat transfer rate is not too high. The most common values assumed for Pr_T are 0.89 or 0.90, in the case of a boundary layer. Heat-transfer predictions can usually be improved somewhat by letting Pr_T vary through the boundary layer. For free shear layers, values of the order of 0.5 are more appropriate for Pr_T .

Molecular Diffusion and Turbulent Transport: If a zero-equation model is used, the $\frac{2}{3}\rho k\delta_{ij}$ contribution in Equation (5.49) is ignored as are the molecular diffusion, $\overline{t_{ji}u_i''}$, and turbulent transport, $\overline{\rho u_j'' \frac{1}{2}u_i'' u_i''}$, terms appearing in the mean-energy equation. Some researchers ignore these terms for higher-order models as well. This is usually a good approximation for flows with Mach numbers up to the supersonic range, which follows from the fact that $\bar{\rho}k \ll P$ (and hence $k \ll \dot{h}$) in most flows of engineering interest. However, at hypersonic speeds, it is entirely possible to achieve conditions under which $\bar{\rho}k$ is a significant fraction of P . To ensure exact conservation of total energy (which includes turbulence kinetic energy), additional closure approximations are needed. The most straightforward procedure for one-equation, two-equation and second-order closure models is to generalize the low-speed closure approximations for the molecular diffusion and turbulent transport terms. The most commonly used approximation is:

$$\overline{t_{ji}u_i''} - \overline{\rho u_j'' \frac{1}{2}u_i'' u_i''} = \left(\mu + \frac{\mu_T}{\sigma_k} \right) \frac{\partial k}{\partial x_j} \quad (5.51)$$

Pressure Diffusion and Pressure-Dilatation Term: Section 4.1 discusses the lack of information regarding diffusion by pressure fluctuations in incompressible flows. So little is known that it is simply ignored. Even less is known for compressible flows. However, given the fundamentally different role that pressure plays in a compressible medium relative to its essentially passive role at low speeds, ignoring pressure diffusion and pressure dilatation ultimately must lead to significant error. Purely empirical proposals, especially for the pressure-dilatation mean product, have been made by many authors, but none has received general acceptance. The best prospect for immediate progress at the present time may be to

use Direct Numerical Simulations (DNS). Such work is in progress [e.g., Sarkar et al. (1991) and Zeman (1991)], and preliminary proposals have been made. No generally accepted approximation has emerged at the time of this writing however.

Pressure Work: The pressure work term, $\overline{u_i'' P_{,i}}$ (or $\overline{u_i'' P_{,j}} + \overline{u_j'' P_{,i}}$ for second-order closure models), arises because the time average of $\overline{u_i''}$ does not vanish. It is proportional to the density/velocity correlation $\overline{\rho' u_i''}$, and illustrates how Favre averaging does not completely eliminate the need to know how these fluctuating properties are correlated. Wilcox and Alber (1972) postulate an empirical model for this term that improves two-equation model predictions for hypersonic base flows. Oh (1974) proposes a closure approximation postulating existence of “eddy shocks” and accurately simulates compressible mixing layers with a one-equation turbulence model. Neither model is entirely satisfactory however as they both involve the mean velocity in a manner that violates Galilean invariance of the Navier-Stokes equation. As with pressure diffusion and pressure dilatation, the best hope for progress in the short term is probably through use of DNS.

5.5 Dilatation Dissipation

Using a program such as MIXER (see Appendix C), it is a simple matter to verify that both the k - ω model and k - ϵ model fail to predict the observed decrease in spreading rate with increasing Mach number for the compressible mixing layer [Kline et al. (1981) and Papamoschou and Roshko (1988)]. Focusing upon the k - ϵ model, Sarkar et al. (1989) and Zeman (1990) have devised particularly elegant models for the k equation that correct the deficiency for the compressible mixing layer. Building upon the Sarkar/Zeman formulations, Wilcox (1992b) has postulated a similar model that enjoys an important advantage for wall-bounded flows. This section shows how a straightforward and elegant modification can dramatically improve a turbulence model’s predictive accuracy.

To understand the Sarkar/Zeman innovation, we must examine the turbulence energy dissipation rate more closely. Recall from Equation (5.38) that

$$\bar{\rho}\epsilon = t_{ji} \overline{\frac{\partial u_i''}{\partial x_j}} \quad (5.52)$$

Hence, in terms of the instantaneous strain-rate tensor, s_{ij} , we have

$$\bar{\rho}\epsilon = \mu \overline{\left[2s_{ji}s_{ij}'' - \frac{2}{3}u_{k,k}u_{i,i}'' \right]} \quad (5.53)$$

Assuming that the correlation between velocity-gradient fluctuations and kinematic viscosity fluctuations is negligible, we can rewrite this equation as

$$\bar{\rho}\epsilon = \bar{\nu} \left[2\overline{\rho s''_{ji} s''_{ij}} - \frac{2}{3}\overline{\rho u''_{k,k} u''_{i,i}} \right] \quad (5.54)$$

In terms of the fluctuating vorticity, ω''_i , there follows

$$\bar{\rho}\epsilon = \bar{\nu} \left[\overline{\rho \omega''_i \omega''_i} + 2\overline{\rho u''_{i,j} u''_{j,i}} - \frac{2}{3}\overline{\rho u''_{i,i} u''_{i,i}} \right] \quad (5.55)$$

Finally, we can say $u''_{i,j} u''_{j,i} \approx (u''_{i,i})^2$, which is exactly true for homogeneous turbulence, and is a very good approximation for high-Reynolds-number, inhomogeneous turbulence [see, for example, Tennekes and Lumley (1983)]. Hence, we conclude that the dissipation can be written as

$$\bar{\rho}\epsilon = \bar{\rho}\epsilon_s + \bar{\rho}\epsilon_d \quad (5.56)$$

where

$$\bar{\rho}\epsilon_s = \bar{\nu} \overline{\rho \omega''_i \omega''_i} \quad \text{and} \quad \bar{\rho}\epsilon_d = \frac{4}{3} \bar{\nu} \overline{\rho u''_{i,i} u''_{i,i}} \quad (5.57)$$

Thus, we have shown that the compressible turbulence dissipation rate can logically be written in terms of the fluctuating vorticity and the divergence of the fluctuating velocity. Equivalently, we could have written the fluctuating velocity as the sum of a divergence free and a curl free component. At high Reynolds number, these components presumably are uncorrelated (again, an exact result for homogeneous turbulence), and Equation (5.55) would follow directly. The quantity ϵ_s is known as the **solenoidal dissipation**, while ϵ_d is known as the **dilatation dissipation**. Clearly, the latter contribution is present only for compressible flows.

Sarkar and Zeman postulate that the dilatation dissipation should be a function of turbulence Mach number, M_t , defined by

$$M_t^2 = 2k/a^2 \quad (5.58)$$

where a is the speed of sound. They argue that the k and ϵ equations should be replaced by

$$\bar{\rho} \frac{dk}{dt} = -\bar{\rho}(\epsilon_s + \epsilon_d) + \dots \quad (5.59)$$

$$\bar{\rho} \frac{d\epsilon_s}{dt} = -C_{\epsilon 2} \bar{\rho} \epsilon_s^2 / k + \dots \quad (5.60)$$

where $C_{\epsilon 2}$ is a closure coefficient. Only the dissipation terms are shown explicitly in Equations (5.59) and (5.60) since no changes occur in any

other terms. Particularly noteworthy, both Sarkar and Zeman postulate that the equation for ϵ_s is unaffected by compressibility. The dilatation dissipation is further assumed to be proportional to ϵ_s so that we say

$$\epsilon_d = \xi^* F(M_t) \epsilon_s \quad (5.61)$$

where ξ^* is a closure coefficient and $F(M_t)$ is a prescribed function of M_t . The Sarkar, Zeman and Wilcox formulations differ in the value of ξ^* and the functional form of $F(M_t)$.

Interestingly, while both Sarkar and Zeman arrive at similar formulations, their basic postulates are fundamentally different. Sarkar et al. postulate that ϵ_d "varies on a fast compressibility time scale relative to ϵ_s ." As a consequence, they conclude that dilatation dissipation increases with M_t in a monotone manner. By contrast, Zeman postulates the existence of eddy shocklets that augment only the dilatation dissipation, so that a threshold exists below which dilatation dissipation is zero.

To implement the Sarkar or Zeman modification in the k - ω model, we begin by making the formal change of variables given by $\epsilon_s = \beta^* \omega k$. This tells us immediately that

$$\bar{\rho} \frac{d\omega}{dt} = \frac{\bar{\rho}}{\beta^* k} \left[\frac{d\epsilon_s}{dt} - \frac{\epsilon_s}{k} \frac{dk}{dt} \right] \quad (5.62)$$

Consequently, a compressibility term must appear in the ω equation as well as in the k equation. Note that if we identify ω as the RMS fluctuating vorticity, a case could be made that the ω equation should be unaffected by dilatation dissipation rather than the ϵ equation. While this may be true, it would obscure direct comparisons between effects of dilatation dissipation on the two types of models if we depart from the Sarkar/Zeman conventions.

Inspection of Equations (4.34) and (4.35) shows that the Sarkar/Zeman compressibility modifications correspond to letting closure coefficients β and β^* in the k - ω model vary with M_t . In terms of ξ^* and the compressibility function $F(M_t)$, β and β^* are:

$$\beta^* = \beta_o^* [1 + \xi^* F(M_t)] \quad (5.63)$$

$$\beta = \beta_o - \beta_o^* \xi^* F(M_t) \quad (5.64)$$

where β_o^* and β_o are the corresponding incompressible values of β^* and β . The values of ξ^* and $F(M_t)$ for the Sarkar, Zeman and Wilcox models are as follows:

Sarkar's Model

$$\xi^* = 1, \quad F(M_t) = M_t^2 \quad (5.65)$$

Zeman's Model

$$\xi^* = 3/4, \quad F(M_t) = \left[1 - e^{-\frac{1}{2}(\gamma+1)(M_t - M_{t_o})^2/\Lambda^2} \right] \mathcal{H}(M_t - M_{t_o}) \quad (5.66)$$

Wilcox's Model

$$\xi^* = 3/2, \quad M_{t_o} = 1/4, \quad F(M_t) = [M_t^2 - M_{t_o}^2] \mathcal{H}(M_t - M_{t_o}) \quad (5.67)$$

where γ is specific heat ratio and $\mathcal{H}(x)$ is the Heaviside step function. Zeman recommends using $\Lambda = 0.60$ and $M_{t_o} = 0.10\sqrt{2/(\gamma+1)}$ for free shear flows. For boundary layers, their values must increase to $\Lambda = 0.66$ and $M_{t_o} = 0.25\sqrt{2/(\gamma+1)}$. Zeman uses a different set of closure coefficients for boundary layers because he postulates that they depend upon the kurtosis, $\overline{u'^4}/(\overline{u'^2})^2$. The kurtosis is presumed to be different for free shear flows as compared to boundary layers. While this is most likely true, it is not much help for two-equation or second-order closure models since such models only compute double correlations and make closure approximations for triple correlations. Quadruple correlations such as $\overline{u'^4}$ are beyond the scope of these models.

To illustrate how well these models perform, we consider mixing of a supersonic stream and a quiescent fluid with constant total temperature. For simplicity, we present results only for the $k-\omega$ model as $k-\epsilon$ results are nearly identical. The equations of motion have been transformed to similarity form for the far field and integrated using Program MIXER, which is described in Appendix C. Figure 5.1 compares computed and measured [see Kline et al. (1981)] spreading rate, C_δ . As in the incompressible case, spreading rate is defined as the difference between the values of y/x where $(U - U_2)^2/(U_1 - U_2)^2$ is 9/10 and 1/10. The quantity C_{δ_o} denotes the incompressible spreading rate and M_c is convective Mach number, viz.,

$$M_c = \frac{U_1 - U_2}{a_1 + a_2} \quad (5.68)$$

Since $U_2 = 0$, Equation (5.68) simplifies to

$$M_c = \frac{M_1}{1 + \left[1 + \frac{(\gamma-1)}{2} M_1^2 \right]^{1/2}} \quad (5.69)$$

As shown, the unmodified $k-\omega$ model fails to predict a significant decrease in spreading rate as Mach number increases. By contrast, the Sarkar, Zeman and Wilcox modifications yield much closer agreement between computed and measured spreading rate.

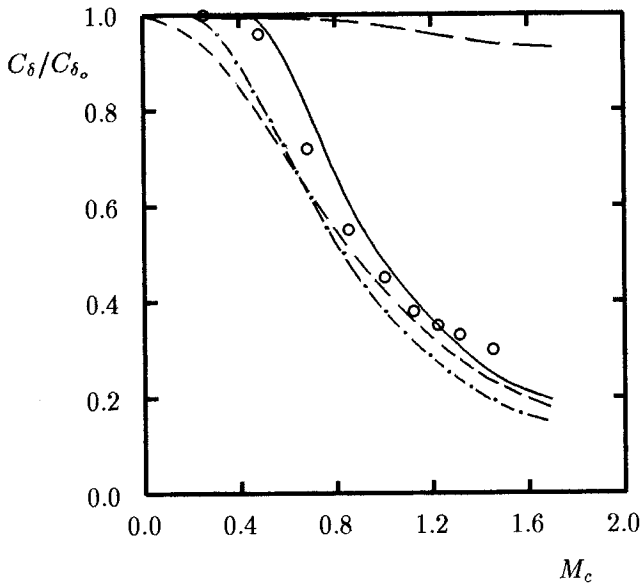


Figure 5.1: Comparison of computed and measured spreading rate for a compressible mixing layer; — — Unmodified $k-\omega$ model; — Wilcox, $\xi^* = 3/2$; - - - Sarkar, $\xi^* = 1$; - · - Zeman, $\xi^* = 3/4$; \circ Langlely curve [Kline et al. (1981)].

We turn now to the adiabatic-wall flat-plate boundary layer. The equations of motion for the $k-\omega$ model have been solved with Program EDDYBL (see Appendix D). Figure 5.2 compares computed skin friction, c_f , with a correlation of measured values for freestream Mach number between 0 and 5. As shown, the unmodified model virtually duplicates measured skin friction. By contrast, the Sarkar compressibility modification yields a value for c_f at Mach 5 that is 18% lower than the value computed with $\xi^* = 0$. Using the Wilcox dilatation-dissipation model yields very little difference in skin friction.

Using $\Lambda = 0.60$ and $M_{t_0} = 0.10\sqrt{2/(\gamma+1)}$ in Zeman's model, computed c_f at Mach 5 is 15% smaller than the value obtained with the unmodified model. Increasing Λ and M_{t_0} to 0.66 and $0.25\sqrt{2/(\gamma+1)}$, respectively, eliminates this discrepancy. However, using this large a value for M_{t_0} for the mixing layer results in discrepancies in excess of 100% between computed and measured spreading rate for M_c in excess of 1.

These results make it clear that neither the Sarkar nor the Zeman compressibility term is completely satisfactory for both the mixing layer and

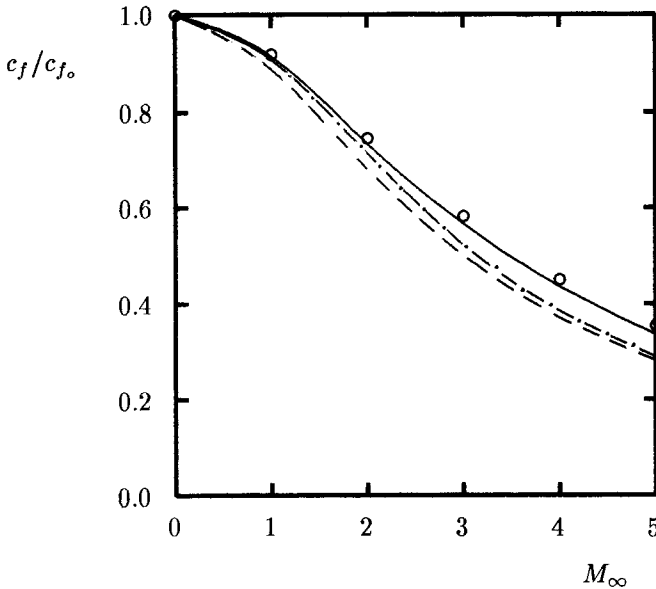


Figure 5.2: Comparison of computed and measured skin friction for a compressible flat-plate boundary layer; — $k-\omega$ with $\xi^* = 0$ and $\xi^* = 3/2$; - - - Sarkar, $\xi^* = 1$; - · - Zeman, $\xi^* = 3/4$; o Van Driest correlation.

boundary layers. The Wilcox dilatation-dissipation model was formulated to resolve this dilemma. Decomposing the dissipation into solenoidal and dilatation components is an important innovation, and is not the root cause of the problem. Rather, the postulated form of the function $F(M_t)$ is the weak link. The Wilcox model provides a satisfactory alternative.

Inspection of the magnitude of turbulence Mach number in mixing layers and boundary layers shows that all is needed is an alternative to the Sarkar and Zeman functional dependencies of ϵ_d upon M_t . Table 5.1 shows why the Sarkar term improves predictions for the mixing layer. The unmodified $k-\omega$ model predicts peak values of M_t in the mixing layer that are more than twice the values in the boundary layer for the same freestream Mach number. Using the Sarkar compressibility term reduces $(M_t)_{max}$ by about one third for the mixing layer when $M_\infty \geq 2$. Even with this much reduction, $(M_t)_{max}$ for the mixing layer remains higher than the largest value of $(M_t)_{max}$ in the boundary layer all the way up to Mach 5.

For Mach 1, the Sarkar term reduces mixing-layer spreading rate below measured values (Figure 5.1). Zeman's term predicts a somewhat larger spreading rate at Mach 1, mainly because of the Mach number threshold in

Table 5.1: Maximum Turbulence Mach Number, $(M_t)_{max}$

M_∞	Boundary Layer		Mixing Layer	
	$\xi^* = 0$	$\xi^* = 1$	$\xi^* = 0$	$\xi^* = 1$
0	0	0	0	0
1	.061	.061	.180	.159
2	.114	.107	.309	.227
3	.149	.135	.384	.245
4	.174	.154	.424	.254
5	.191	.171	.453	.266

Zeman's model. That is, Zeman postulates that the compressibility effect is absent for $M_t < M_{t_0}$. Zeman's Mach number threshold also yields smaller differences between computed and measured boundary-layer skin friction at lower Mach numbers (see Figure 5.2). These observations show that an improved compressibility term can be devised by extending Zeman's threshold Mach number to a larger value of M_t . The Wilcox model simply combines the relative simplicity of Sarkar's functional form for $F(M_t)$ with Zeman's Mach number threshold to accomplish this end.

5.6 Compressible Law of the Wall

In this section, we use perturbation methods to examine k - ω and k - ϵ model predicted, compressible log-layer structure. The results are particularly illuminating and clearly demonstrate why the Sarkar and Zeman compressibility terms adversely affect boundary-layer predictions.

Recall from Section 4.6.1 that the log layer is the region sufficiently close to the solid boundary for neglect of convective terms and far enough distant for molecular diffusion terms to be dropped. In the log layer, the equations of motion based on the k - ω model simplify to the following.

$$\mu_T \frac{d\tilde{u}}{dy} = \bar{\rho}_w u_\tau^2 \quad (5.70)$$

$$\mu_T \frac{d}{dy} \left[\frac{C_p \tilde{T}}{Pr_T} + \frac{1}{2} \tilde{u}^2 + \sigma^* k \right] = -q_w \quad (5.71)$$

$$\sigma^* \frac{d}{dy} \left[\mu_T \frac{dk}{dy} \right] + \mu_T \left(\frac{d\tilde{u}}{dy} \right)^2 - \beta^* \bar{\rho} \omega k = 0 \quad (5.72)$$

$$\sigma \frac{d}{dy} \left[\mu_T \frac{d\omega}{dy} \right] + \alpha \bar{\rho} \left(\frac{d\tilde{u}}{dy} \right)^2 - \beta \bar{\rho} \omega^2 = 0 \quad (5.73)$$

$$\bar{\rho} \tilde{T} = \bar{\rho}_w \tilde{T}_w \quad (5.74)$$

The quantity u_τ is friction velocity defined as $\sqrt{\tau_w / \bar{\rho}_w}$ where τ_w is surface shear stress and $\bar{\rho}_w$ is density at the surface. Also, \tilde{T}_w is surface temperature, q_w is surface heat flux and C_p is specific heat at constant pressure. Finally, y is distance from the surface.

Following Saffman and Wilcox (1974), we change independent variables from y to \tilde{u} . Consequently, derivatives transform according to

$$\mu_T \frac{d}{dy} = \mu_T \frac{d\tilde{u}}{dy} \frac{d}{d\tilde{u}} = \bar{\rho}_w u_\tau^2 \frac{d}{d\tilde{u}} \quad (5.75)$$

With this change of variables, we replace Equations (5.71)-(5.73) by the following.

$$\frac{d}{d\tilde{u}} \left[\frac{C_p \tilde{T}}{Pr_T} + \frac{1}{2} \tilde{u}^2 + \sigma^* k \right] = - \frac{q_w}{\bar{\rho}_w u_\tau^2} \quad (5.76)$$

$$\sigma^* \frac{d^2 k}{d\tilde{u}^2} + 1 - \frac{\beta^* \bar{\rho}^2 k^2}{\bar{\rho}_w^2 u_\tau^4} = 0 \quad (5.77)$$

$$\sigma \frac{d^2 \omega}{d\tilde{u}^2} + \alpha \frac{\omega}{k} - \frac{\beta \bar{\rho}^2 k \omega}{\bar{\rho}_w^2 u_\tau^4} = 0 \quad (5.78)$$

Integrating Equation (5.76) yields the temperature, and hence the density, as a function of velocity and Mach number based on friction velocity, $M_\tau \equiv u_\tau / a_w$.

$$\frac{\tilde{T}}{\tilde{T}_w} = \frac{\bar{\rho}_w}{\bar{\rho}} = 1 - (\gamma - 1) Pr_T M_\tau^2 \left[\frac{1}{2} \left(\frac{\tilde{u}}{u_\tau} \right)^2 + \frac{q_w}{\bar{\rho}_w u_\tau^3} \left(\frac{\tilde{u}}{u_\tau} \right) + \sigma^* \left(\frac{k}{u_\tau^2} \right) \right] \quad (5.79)$$

Next, we assume a solution of the form:

$$\bar{\rho} k = \Gamma \bar{\rho}_w u_\tau^2 \quad (5.80)$$

where Γ is a constant to be determined. Substituting Equations (5.79) and (5.80) into Equation (5.77), and noting that $M_i^2 = 2\Gamma M_\tau^2$, leads to the following quartic equation for Γ .

$$\beta_o^* [1 + 2\xi^* M_\tau^2 \Gamma] [1 + (\gamma - 1)Pr_T \sigma^* M_\tau^2 \Gamma] \Gamma^2 = 1 \quad (5.81)$$

As can easily be verified, when $M_\tau^2 \ll 1$, the asymptotic solution for Γ is

$$\Gamma = \frac{1}{\sqrt{\beta_o^*}} - \left[\frac{\xi^* + \frac{(\gamma-1)}{2} Pr_T \sigma^*}{\beta_o^*} \right] M_\tau^2 + \dots \quad (5.82)$$

Finally, in terms of Γ , Equation (5.78) simplifies to

$$\sigma \frac{d^2 \omega}{d\tilde{u}^2} + \{ \alpha - [\beta_o - 2\beta_o^* \xi^* M_\tau^2 \Gamma] \Gamma^2 \} \frac{\bar{\rho} \omega}{\bar{\rho}_w u_\tau^2 \Gamma} = 0 \quad (5.83)$$

Combining Equations (5.79) and (5.80) yields the density as a function of velocity and Γ .

$$\frac{\bar{\rho}_w}{\bar{\rho}} = \frac{1 - \frac{(\gamma-1)}{2} Pr_T M_\tau^2 \left[\left(\frac{\tilde{u}}{u_\tau} \right)^2 + \frac{2q_w}{\rho_w u_\tau^3} \left(\frac{\tilde{u}}{u_\tau} \right) \right]}{1 + (\gamma - 1) Pr_T \sigma^* \Gamma M_\tau^2} \quad (5.84)$$

Equation (5.84) assumes a more compact form if we introduce the freestream velocity, U_∞ . A bit more algebra yields

$$\frac{\bar{\rho}_w}{\bar{\rho}} = \frac{1 + Bv - A^2 v^2}{1 + (\gamma - 1) Pr_T \sigma^* \Gamma M_\tau^2} \quad (5.85)$$

where

$$\left. \begin{aligned} v &= \tilde{u}/U_\infty \\ A^2 &= \frac{(\gamma-1)}{2} Pr_T M_\infty^2 (\tilde{T}_\infty/\tilde{T}_w) \\ B &= -Pr_T q_w U_\infty / (C_p \tilde{T}_w \tau_w) \end{aligned} \right\} \quad (5.86)$$

Using Equations (5.82), (5.85) and (5.86), and retaining terms up to $O(M_\tau^2)$, Equation (5.83) assumes the following form,

$$\frac{d^2 \omega}{dv^2} - \left[\frac{K_\omega^2 (U_\infty/u_\tau)^2}{1 + Bv - A^2 v^2} \right] \omega = 0 \quad (5.87)$$

where the constant K_ω is defined by

$$K_\omega^2 = \kappa^2 - \left[\frac{(2 + \alpha + \beta_o/\beta_o^*)\xi^*}{\sigma} + \frac{(\gamma - 1)Pr_T(3\alpha - \beta_o/\beta_o^*)\sigma^*}{2\sigma} \right] M_\tau^2 + \dots \quad (5.88)$$

and κ is Kármán's constant. Because $U_\infty/u_\tau \gg 1$, we can use the WKB method [see Kevorkian and Cole (1981)] to solve Equation (5.87). Noting that ω decreases as \tilde{u}/U_∞ increases, the asymptotic solution for ω is

$$\omega \sim C [1 + Bv - A^2v^2]^{1/4} \exp[-K_\omega u^*/u_\tau] \quad (5.89)$$

where C is a constant of integration and u^* is defined by

$$\frac{u^*}{U_\infty} = \frac{1}{A} \sin^{-1} \left(\frac{2A^2v - B}{\sqrt{B^2 + 4A^2}} \right) \quad (5.90)$$

Combining Equations (5.70), (5.80) and (5.89), we can relate velocity and distance from the surface.

$$\int [1 + Bv - A^2v^2]^{-1/4} \exp[K_\omega u^*/u_\tau] dv \sim \frac{Cy}{\Gamma U_\infty} \quad (5.91)$$

We integrate by parts to generate the asymptotic expansion of the integral in Equation (5.91) as $U_\infty/u_\tau \rightarrow \infty$. Hence,

$$[1 + Bv - A^2v^2]^{1/4} \exp[K_\omega u^*/u_\tau] \sim \frac{K_\omega Cy}{\Gamma u_\tau} \quad (5.92)$$

Finally, we set the constant of integration $C = \Gamma u_\tau^2 / (K_\omega \nu_w)$. Taking the natural log of Equation (5.92), we conclude that

$$\frac{u^*}{u_\tau} \sim \frac{1}{K_\omega} \ln \left(\frac{u_\tau y}{\nu_w} \right) + B_\omega \quad (5.93)$$

The quantity B_ω is the effective "constant" in the law of the wall defined by

$$B_\omega = B + \frac{1}{K_\omega} \ln \left(\frac{\bar{\rho}}{\bar{\rho}_w} \right)^{1/4} \quad (5.94)$$

where B is a true constant.

Most of the analysis above holds for the k - ϵ model. The only significant difference is in the ϵ equation which is as follows.

$$\sigma_\epsilon^{-1} \frac{d}{dy} \left[\mu_T \frac{d\epsilon}{dy} \right] + C_\mu C_{\epsilon 1} \bar{\rho} k \left(\frac{d\tilde{u}}{dy} \right)^2 - C_{\epsilon 2} \frac{\bar{\rho} \epsilon^2}{k} = 0 \quad (5.95)$$

Equations (5.80), (5.82) and (5.85) are still valid for the turbulence kinetic energy and density, provided σ^* is replaced by σ_k^{-1} . The transformed equation for ϵ is

$$\frac{d^2 \epsilon}{dv^2} - \left[\frac{K_\epsilon^2 (U_\infty/u_\tau)^2}{1 + Bv - A^2v^2} \right] \epsilon = 0 \quad (5.96)$$

where the constant K_ϵ is defined by

$$K_\epsilon^2 = \kappa^2 - \left[(C_{\epsilon 1} + C_{\epsilon 2}) \sigma_\epsilon \xi^* + \frac{(\gamma - 1) Pr_T (3C_{\epsilon 1} - C_{\epsilon 2}) \sigma_\epsilon}{2\sigma_k} \right] M_\tau^2 + \dots \quad (5.97)$$

In arriving at Equation (5.97), recall from Equation (4.106) that the k - ϵ model's closure coefficients are related by

$$\kappa^2 = \sqrt{C_\mu} (C_{\epsilon 2} - C_{\epsilon 1}) \sigma_\epsilon \quad (5.98)$$

The asymptotic solution for ϵ is

$$\epsilon \sim C [1 + Bv - A^2 v^2]^{1/4} \exp[-K_\epsilon u^*/u_\tau] \quad (5.99)$$

Velocity and distance from the surface are related by

$$\int [1 + Bv - A^2 v^2]^{3/4} \exp[K_\epsilon u^*/u_\tau] dv \sim C_0 y \quad (5.100)$$

where C_0 is a constant of integration. Consequently, Equation (5.92) is replaced by

$$[1 + Bv - A^2 v^2]^{5/4} \exp[K_\epsilon u^*/u_\tau] \sim C_1 y \quad (5.101)$$

where C_1 is another constant of integration. Finally, the law of the wall for the k - ϵ model is

$$\frac{u^*}{u_\tau} \sim \frac{1}{K_\epsilon} \ell n \left(\frac{u_\tau y}{\nu_w} \right) + B_\epsilon \quad (5.102)$$

where B_ϵ is given by

$$B_\epsilon = B + \frac{1}{K_\epsilon} \ell n \left(\frac{\bar{\rho}}{\bar{\rho}_w} \right)^{5/4} \quad (5.103)$$

Equations (5.93) and (5.102) are very similar to the compressible law of the wall deduced by Van Driest (1951). There are two ways in which these equations differ from the Van Driest law.

The first difference is the effective Kármán constants, K_ω and K_ϵ , which vary with M_τ according to Equation (5.88) for the k - ω model and Equation (5.97) for the k - ϵ model. In terms of each model's closure coefficients, K_ω and K_ϵ are given by (for $M_\tau \ll 1$):

$$K_\omega^2 \sim \kappa^2 [1 - (40.29\xi^* + 0.87)M_\tau^2 + \dots] \quad (5.104)$$

and

$$K_\epsilon^2 \sim \kappa^2 [1 - (23.92\xi^* + 3.07)M_\tau^2 + \dots] \quad (5.105)$$

Table 5.2: Effective Kármán Constant

M_∞	$M_\tau _{\xi^*=0}$	K_ω	$M_\tau _{\xi^*=1}$	K_ω
0	0	.410	0	.410
1	.032	.410	.031	.402
2	.048	.410	.046	.392
3	.052	.410	.049	.389
4	.050	.410	.046	.392
5	.048	.410	.043	.394

Table 5.2 summarizes results obtained in the boundary-layer computations of Section 5.5 for the unmodified k - ω model ($\xi^* = 0$) and for the k - ω model with the Sarkar compressibility term ($\xi^* = 1$). The value of K_ω for the unmodified model deviates from the Kármán constant, $\kappa = 0.41$, by less than 0.12% for freestream Mach numbers between 0 and 5. By contrast, when $\xi^* = 1$, the deviation is as much as 5.10%. This large a deviation in the effective Kármán constant is consistent with the observed differences between computed and measured skin friction. Similarly, with $M_\tau = .05$, K_ϵ differs from κ by 0.5% and 3.5% for $\xi^* = 0$ and 1, respectively. Thus the Sarkar compressibility term has a somewhat smaller effect on κ for the k - ϵ model relative to the effect on κ for the k - ω model.

To see why a small perturbation in κ corresponds to a larger perturbation in c_f , differentiate the law of the wall with respect to κ . Noting that $c_f = \frac{1}{2}u_\tau^2/U_\infty^2$, a little algebra shows that

$$\frac{dc_f}{d\kappa} \approx \frac{2}{\kappa}c_f \quad (5.106)$$

Thus, we should expect $\Delta c_f/c_f$ to be double the value of $\Delta\kappa/\kappa$. The numerical results indicate somewhat larger differences in c_f , but the trend is clear.

The second way Equations (5.93) and (5.102) differ from the Van Driest compressible law of the wall is in the effective variation of the “constant” terms B_ω and B_ϵ with $(\bar{\rho}/\bar{\rho}_w)$. Because the exponent is only 1/4, the effect is minor for the k - ω model. By contrast, the exponent is 5/4 for the k - ϵ model. This large an exponent has a much stronger effect on predicted boundary layer properties. Figure 5.3 compares computed and measured [Fernholz and Finlay (1981)] velocity profiles for adiabatic-wall boundary layers at Mach numbers 4.5 and 10.3. The computed results are for the Wilcox (1988a) k - ω model and for Chien’s (1982) low-Reynolds-number

k - ϵ model. Equations (5.93) and (5.102) are also shown (with $B = 5.0$) to underscore the importance of the models' variable "constant" in the compressible law of the wall.

These results are consistent with the analysis of Huang, Bradshaw and Coakley (1992) that shows how poorly the k - ϵ model performs for compressible boundary layers. Since $\bar{\rho}/\bar{\rho}_w > 1$ for all but strongly cooled walls, its effect is to increase the "constant" in the law of the wall with a corresponding decrease in c_f . The Sarkar and Zeman terms will thus amplify this inherent deficiency of the k - ϵ model.

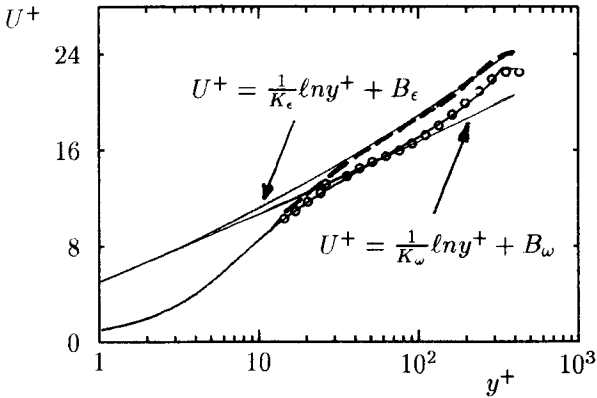
To put these results in proper perspective, we must not lose sight of the fact that the k - ϵ model requires the use of either wall functions or viscous damping functions in order to calculate wall-bounded flows. If these functions have an effect that persists well into the log layer, it may be possible to suppress the k - ϵ model's inherent flaws at low Reynolds numbers. However, the perturbation analysis shows that such a model will not be asymptotically consistent with the compressible law of the wall in the limit of infinite Reynolds number. In effect, such a model would have compensating errors that may fortuitously yield reasonably close agreement with the law of the wall at low Reynolds numbers.

As a final comment, if we had used $\rho\epsilon$ as the dependent variable in Equation (5.95) in place of ϵ , the exponent $5/4$ in Equation (5.103) would be reduced to $1/4$. Presumably, this change would improve k - ϵ model predictions for compressible boundary layers. The effect of this rescaling on the mixing layer is unclear.

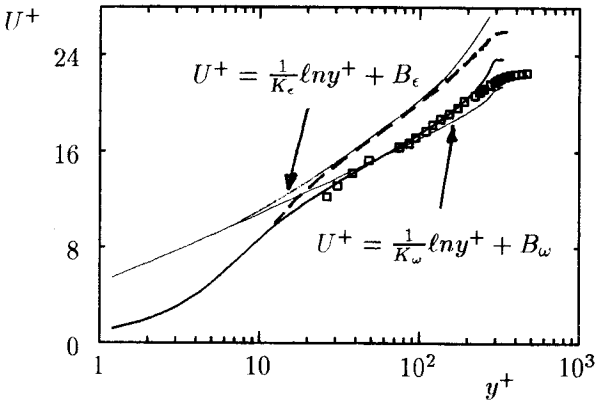
5.7 Compressible Boundary Layers

Most turbulence models are capable of providing reasonably accurate predictions for constant-pressure, adiabatic-wall boundary layers provided the Mach number does not exceed about 5. Similar to the incompressible situation, adverse pressure gradients continue to be anathema to the k - ϵ model, while presenting no major problem for the k - ω model. When surface heat transfer is present, model predictions often show nontrivial discrepancies from measured values for most turbulence models.

Algebraic models such as the Cebeci-Smith and Baldwin-Lomax models (see Subsections 3.4.1 and 3.4.2) require no special compressibility corrections. For the sake of clarity, recall that the Cebeci-Smith model uses the velocity thickness, δ_v^* , defined in Equation (3.115) for both compressible and incompressible flow. The velocity thickness differs from the displacement



(a) Mach 4.5



(b) Mach 10.3

Figure 5.3: Comparison of computed and measured velocity profiles for compressible flat-plate boundary layers; — Wilcox $k-\omega$; - - - Chien $k-\epsilon$; \circ Coles; \square Watson.

thickness, δ^* , which is defined for compressible flows by

$$\delta^* = \int_0^\infty \left(1 - \frac{\bar{\rho}}{\rho_e} \frac{\tilde{u}}{\tilde{u}_e} \right) dy \quad (5.107)$$

The primary reason algebraic models should fare well for compressible boundary layers without special compressibility modifications is illustrated by Maise and McDonald (1967). Using the best experimental data of the time for compressible boundary layers, they inferred the mixing length variation. Their analysis shows that for Mach numbers up to 5:

- Velocity profiles for adiabatic walls correlate with the incompressible profile when the Van Driest (1951) scaling is used, i.e.,

$$\frac{u^*}{U_\infty} = \frac{1}{A} \sin^{-1} \left(A \frac{\tilde{u}}{U_\infty} \right), \quad A^2 = \frac{(\gamma - 1)}{2} M_\infty^2 (\tilde{T}_\infty / \tilde{T}_w) \quad (5.108)$$

- The Van Driest scaling fails to correlate compressible velocity profiles when surface heat transfer is present.
- The classical mixing length is independent of Mach number.

Using singular perturbation methods, Barnwell (1992) shows that algebraic models are consistent with the Maise-McDonald observations. Many researchers have applied the Cebeci-Smith model to compressible boundary layers, showing excellent agreement with measurements for adiabatic walls and somewhat larger differences when surface heat transfer is present. The Baldwin-Lomax model yields similar predictions.

Because the length scale employed in most one-equation models is patterned after the mixing length, they should also be expected to apply to compressible flows without ad hoc compressibility modifications. This is indeed the case, especially for newer models, which have been designed for compressible-flow applications. Figure 4.2, for example, shows how the Baldwin-Barth (1990) model performs for a Mach 2 flat-plate boundary layer.

As we have seen in the last subsection, the issue is more complicated for two-equation models. The log-layer solution indicates that the length scale for the k - ω and k - ϵ models varies linearly with distance from the surface, independent of Mach number. The models even predict the Van Driest velocity scaling. Thus, two-equation models are consistent with two of the most important observations made by Maise and McDonald, at least in the log layer. However, we have also seen that the ϵ equation includes a nonphysical density effect that distorts the model's log-layer structure, and precludes a satisfactory solution. By contrast, the ω equation is entirely

consistent with the Maise-McDonald observations. As shown in Figures 5.2 and 5.3, the k - ω model provides excellent quantitative agreement with measurements for Mach numbers up to about 5.

Turning to effects of pressure gradient, Figures 5.4 and 5.5 compare computed and measured skin friction and velocity profiles for two compressible boundary layers with adverse pressure gradient. Figure 5.4 corresponds to a Mach 4, adiabatic-wall experiment conducted by Zwarts [see Kline et al. (1981) — Flow 8411]. Computed results are shown for the Wilcox k - ω model without viscous corrections and for the Chien (1982) k - ϵ model. Although the effect is small for this flow, neither computation includes a dilatation-dissipation correction. As shown, k - ω model predictions fall within the scatter of the experimental data. By contrast, the k - ϵ model skin friction is about 8% lower than measured at the beginning of the computation where the Mach number is 4. This is consistent with results shown in Figure 5.3(a). Because the flow is decelerating, the Mach number decreases with distance, and falls to 3 by the end of the run. As a result, $\bar{\rho}_e/\bar{\rho}_w$ is only half its upstream value, and the corresponding distortion of the k - ϵ model's log-layer velocity profile is greatly reduced. Consequently, the k - ϵ model's velocity profile is fortuitously in close agreement with the measured profile.

Figure 5.5 presents a similar comparison for a Mach 2.65 boundary layer with adverse pressure gradient and mild surface heating. The ratio of wall temperature to the adiabatic-wall temperature, T_w/T_{aw} , varies between 1.07 and 1.13 for the flow. Again, because the Mach number is in the low supersonic range, the density term in the k - ϵ model's law of the wall is small. The value of $K_\epsilon^{-1} \ell n(\bar{\rho}/\bar{\rho}_w)^{5/4}$ ranges between 0.50 at $y^+ = 100$ to 1.45 at $y^+ = 5000$. By comparison, the distortion in the k - ω model's law of the wall is just a fifth of these values.

While the k - ϵ model solutions for both of these adverse pressure gradient cases are nearly as close to measurements as the k - ω model solutions, similar results should not be expected for higher Mach numbers. Many compressible-flow experiments have been conducted for Mach numbers of 3 and less. Far fewer experiments have been done at higher Mach numbers. Hence these results show how a model calibrated for the best data available may not apply at higher Mach numbers.

The k - ϵ model's near-wall behavior has a significant impact on model predictions, and Chien's model happens to be optimum for these two flows. The Jones-Launder (1972) and Launder-Sharma (1974) models, for example, predict skin friction values more than twice measured values for these two flows. Zhang et al. (1992) have developed a low-Reynolds-number k - ϵ model that yields close agreement with constant-pressure boundary layer data for Mach numbers up to 10. Interestingly, they note from the work

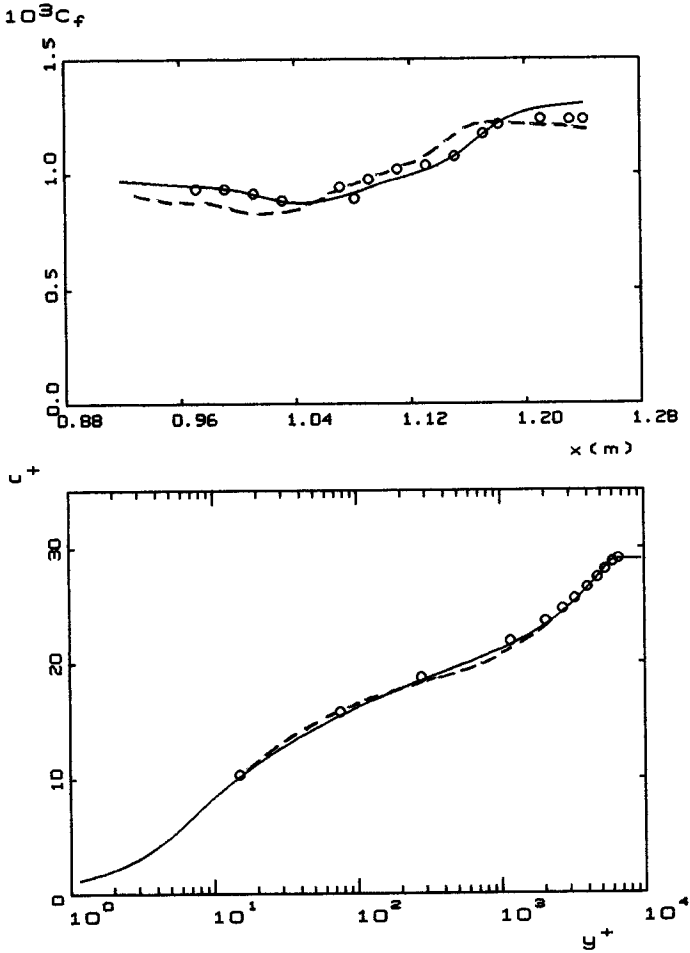


Figure 5.4: Computed and measured skin friction and velocity profile (at $x = 1.18$ m.) for a Mach 4, adiabatic-wall boundary layer with an adverse pressure gradient; — $k-\omega$ model; - - - Chien $k-\epsilon$ model; o Zwarts.

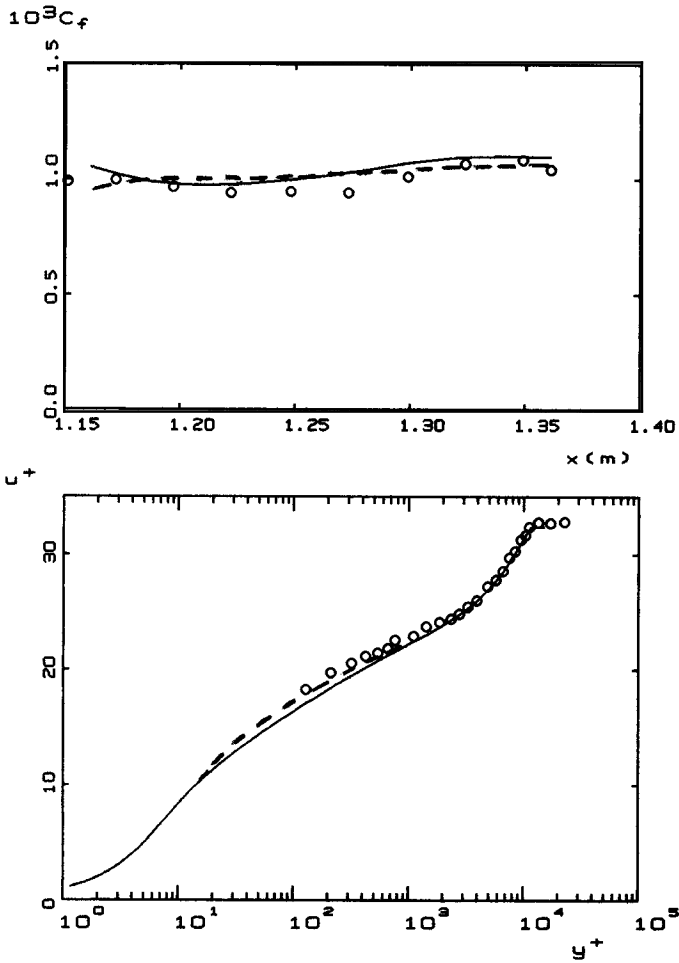


Figure 5.5: Computed and measured flow properties for a Mach 2.65, heated-wall boundary layer with an adverse pressure gradient; — $k-\omega$ model; - - - Chien $k-\epsilon$ model; \circ Fernando and Smits.

of Coleman and Mansour (1991) that the exact Favre-averaged equation for solenoidal dissipation, ϵ_s , includes a term proportional to the rate of change of the kinematic viscosity, $\bar{\nu}$, as follows:

$$\bar{\rho} \frac{d\epsilon_s}{dt} = \frac{\bar{\rho}\epsilon_s}{\bar{\nu}} \frac{d\bar{\nu}}{dt} + \dots \quad (5.109)$$

which can be rewritten as

$$\bar{\rho}\bar{\nu} \frac{d}{dt} \left(\frac{\epsilon_s}{\bar{\nu}} \right) = \dots \quad (5.110)$$

This corresponds to an effective change of dependent variable in the ϵ_s equation. Assuming a power-law viscosity law, i.e., $\bar{\mu} \propto \tilde{T}^n$, the effective rescaled dependent variable would be $\bar{\rho}^{(1+n)}\epsilon_s$. Correspondingly, the exponent 5/4 in Equation (5.103) would become $(n + 1/4)$. For a typical value $n = 7/10$, the new coefficient would be 0.95. Hence this term should yield only a slight improvement for the model's distorted law of the wall. Actually, through a series of closure approximations, Zhang et al. combine this term with other terms and arrive at a rescaling that effectively leads to using $\bar{\rho}^{-0.61}\epsilon_s$. This would correspond to replacing the exponent 5/4 by 1.86 which would yield even more distortion. It is unclear how Zhang et al. have circumvented the inherent flaw in the k - ϵ model for compressible flows. Since virtually all of their applications to date have been for low-Reynolds-number flows, it is possible that their low-Reynolds-number damping functions penetrate far enough above the sublayer to offset the behavior indicated in Equation (5.103).

Turning to effects of surface heat transfer, Figure 5.6 compares computed skin friction with a correlation of measured values [see Kline, et al. (1981) — Flow 8201]. As shown, the k - ω model virtually duplicates the Van Driest correlation, although noticeable differences appear when wall temperature is reduced to one fifth of the adiabatic-wall temperature. The k - ϵ model predictions of Zhang et al. (1992) show a similar trend.

As the final application, consider compressible flow over roughened flat plates. Note that this provides a test of the k - ω model rough-surface boundary condition on flows for which it has not been calibrated. Figure 5.7 compares computed skin friction with the data summarized by Reda, Ketter and Fan (1974). Computations have been done for Mach numbers of 0, 1 and 5 and dimensionless roughness height, k_R^+ , ranging from 0 to 100. For each Mach number, the reference smooth-wall skin friction coefficient, c_{f_o} , corresponds to a momentum-thickness Reynolds number, Re_θ , of 10,000. As shown, computed skin friction falls well within experimental data scatter.

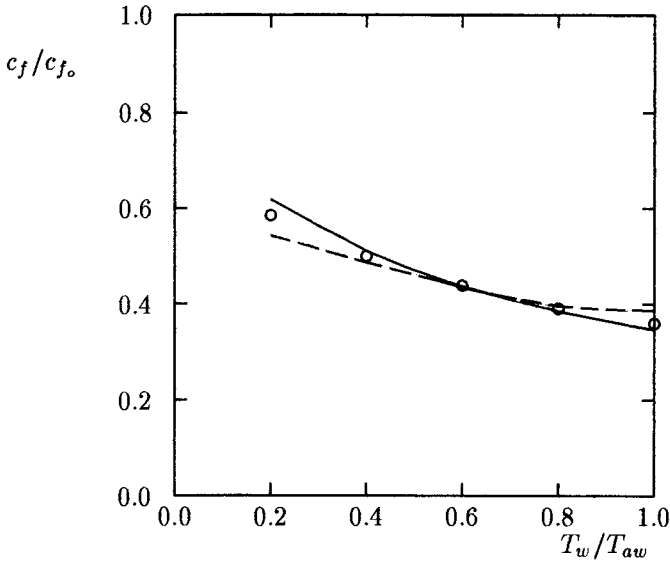


Figure 5.6: Computed and measured effects of surface cooling on skin friction for a Mach 5 flat-plate boundary layer; — $k-\omega$ model; - - - Zhang et al. $k-\epsilon$ model; \circ Van Driest correlation.

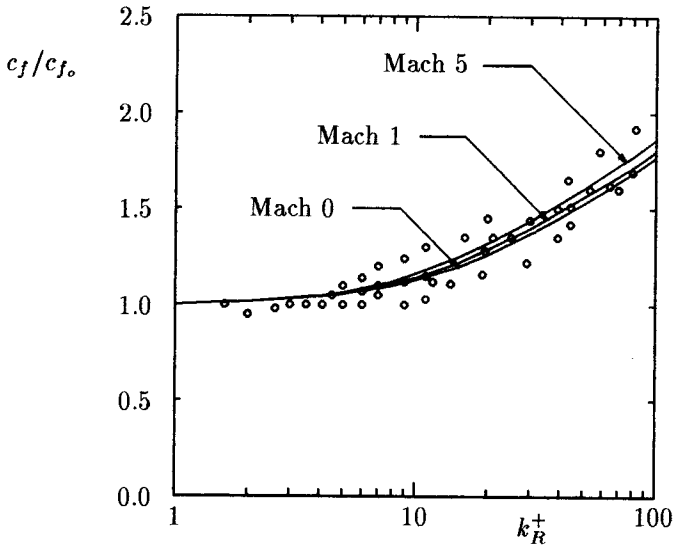


Figure 5.7: Computed and measured effects of surface roughness on skin friction for compressible flat-plate boundary layers; — $k-\omega$ model; \circ Reda, Ketter and Fan.

The computations also demonstrate consistency with the observation originally made by Goddard (1959) that “the effect of surface roughness on skin-friction drag is localized deep within the boundary layer at the surface itself and is independent of the external flow, i.e., Mach number, per se, is eliminated as a variable.” Consistent with Goddard’s observation, Mach number has little effect on predicted c_f/c_{f_0} . Additionally, consistent with Reda’s findings, computed skin friction departs noticeably from the smooth-wall value for k_R^+ values near 4 to 5 as opposed to Goddard’s correlation which indicates no effect for k_R^+ less than 10.

5.8 Shock-Induced Boundary-Layer Separation

One of the most interesting and challenging CFD problems is the interaction of a turbulent boundary layer with a shock wave. Many researchers have analyzed this problem since the 1960’s, with varying degrees of success. The earliest efforts were confined to algebraic models, largely because of the long computing times required to solve the full Favre-averaged Navier-Stokes equation. The fastest computer of the late 1960’s and early 1970’s was the CDC 7600, a machine comparable in speed to a 50 MHz 80486 based microcomputer. Additionally, the best compressible-flow numerical algorithms of that era were explicit time-marching methods that required tens of thousands of timesteps to achieve a solution.

Wilcox (1974) did the first solutions to the Favre-averaged Navier-Stokes equation, using an advanced turbulence model, for shock-induced separation of a turbulent boundary layer. This early CFD study included six computations, three for reflection of an oblique shock from a flat plate and three for flow into a compression corner. Results of the study indicate that, using a two-equation turbulence model, a reasonably accurate description of the flowfield can be obtained for reflection of an oblique shock from a flat plate. However, the numerical flowfields for the compression corner cases differ significantly from the experimentally observed flowfields, even though Mach and Reynolds numbers and shock strength are identical to those of the flat-plate cases. Thus, a seemingly simple change in flow geometry causes a major difference in predictive accuracy. To put these computations in proper perspective, note that the turbulence model used was the Saffman-Wilcox (1974) $k-\omega^2$ model with surface boundary conditions given by matching to the law of the wall. The numerical algorithm used was a first-order accurate explicit time-marching procedure.

Since that time, computational methods have improved dramatically

thanks to the innovative work of many researchers such as Beam and Warming (1976), Steger and Warming (1979), Roe (1981), Van Leer (1982), MacCormack (1985), and Roache and Salari (1990), to name just a few. As a result of their innovations, converged solutions for separated flows can often be obtained in less than 200 timesteps. A two-equation turbulence model computation now takes about two hours of 80486-based microcomputer CPU time for a shock-separated flow.

While great advances have been made in developing accurate and efficient finite difference algorithms, far less improvement has been made with turbulence models for such flows. The work of Viegas and Horstman (1979), Viegas, Rubesin and Horstman (1985), Champney (1989) and Horstman (1992) provides clear substantiation of this claim. They have applied many turbulence models to shock-separated flows with almost universal results, viz.:

1. too little upstream influence as shown by pressure starting to rise well downstream of the measured beginning of adverse pressure gradient;
2. surface pressure in excess of measured values in the region directly above the separation bubble;
3. skin friction and heat transfer higher than measured downstream of reattachment;
4. velocity profiles downstream of reattachment that indicate flow deceleration in excess of corresponding measurements.

On the one hand, by using wall functions and the $k-\epsilon$ model, Viegas, Horstman and Rubesin (1985) are able to remove Item 3 from this list. On the other hand, they achieve only modest improvements in the other items. This lack of success on the compression-corner problem, which has persisted for more than a decade, is excellent testimony to the oft quoted statement that **turbulence modeling is the pacing item in CFD**.

Most modern shock-separated computations are done without introducing wall functions. There is no evidence that the law of the wall holds on separated regions, and its use via wall functions is a questionable approximation. The primary motivation for using wall functions in large scale computations that require substantial computer resources is in reducing CPU time. Viegas, Horstman and Rubesin (1985), in effect, create a two-layer turbulence model where their wall functions apply in the sublayer, and the Standard $k-\epsilon$ model applies above the sublayer. While their procedure yields significant reduction in computing time, numerical results are sensitive to the location of the grid point closest to the surface, y_2^+ . In fact, there is no obvious convergence to a well defined limiting value as $y_2^+ \rightarrow 0$.

Consequently, the value of y_2^+ is effectively an adjustable parameter in their model equations, to be selected by the user. In practice, it is typical for the user to fix y_2 at each location, rather than modify it locally as the solution develops, which would be required to achieve a constant value of y_2^+ . Thus, in practice, y_2^+ actually varies throughout the flow in a manner that cannot be determined a priori, so that the sensitivity to its value is a computational liability.

The sensitivity can be removed by using perturbation methods to devise suitable wall functions. Wilcox (1989), for example, has deduced the following compressible-flow wall functions for the k - ω model:

$$\left. \begin{aligned} u^* &= u_\tau \left[\frac{1}{\kappa} \ln \left(\frac{u_\tau y}{\nu_w} \right) + B - 0.48 \frac{u_\tau y}{\nu_w} \phi + O(\phi^2) \right] \\ k &= \frac{\bar{\rho}_w}{\bar{\rho}} \frac{u_\tau^2}{\sqrt{\beta^*}} \left[1 + 1.16 \frac{u_\tau y}{\nu_w} \phi + O(\phi^2) \right] \\ \omega &= \sqrt{\frac{\bar{\rho}_w}{\bar{\rho}}} \frac{u_\tau}{\sqrt{\beta^*} \kappa y} \left[1 - 0.32 \frac{u_\tau y}{\nu_w} \phi + O(\phi^2) \right] \end{aligned} \right\} \quad (5.111)$$

where ϕ is the dimensionless pressure gradient parameter defined by

$$\phi = \frac{\nu_w}{\rho u_\tau^3} \frac{dP}{dx} \quad (5.112)$$

As with the incompressible wall functions deduced for the incompressible k - ω model (see Subsection 4.7.1), the expansions in Equation (5.111) have been derived assuming ϕ is a small parameter. Using these wall functions, numerical solutions show very little sensitivity to placement of the grid point closest to the surface.

Figure 5.8 compares computed and measured surface pressure for Mach 3 flow into a 24° compression corner using algebraic models, a one-equation model, several two-equation models, and a second-order closure model. As shown, none of the algebraic, one-equation or two-equation models provides a satisfactory solution. Figure 5.9 illustrates a critical problem regarding prediction of surface heating rates. Results are shown for three k - ϵ models, viz., the Jones-Launder (1972) model, the same model with compressibility corrections devised by Rubesin (1990), and a two-layer k - ϵ model developed by Rodi (1991) that uses a one-equation model rather than wall functions. As shown, the Jones-Launder model surface heat transfer, q_w , is off scale and is roughly triple the measured value. While the modified models predict peak heating rates closer to measured values, differences between computed and measured heat transfer are in excess of 25% throughout the flow.

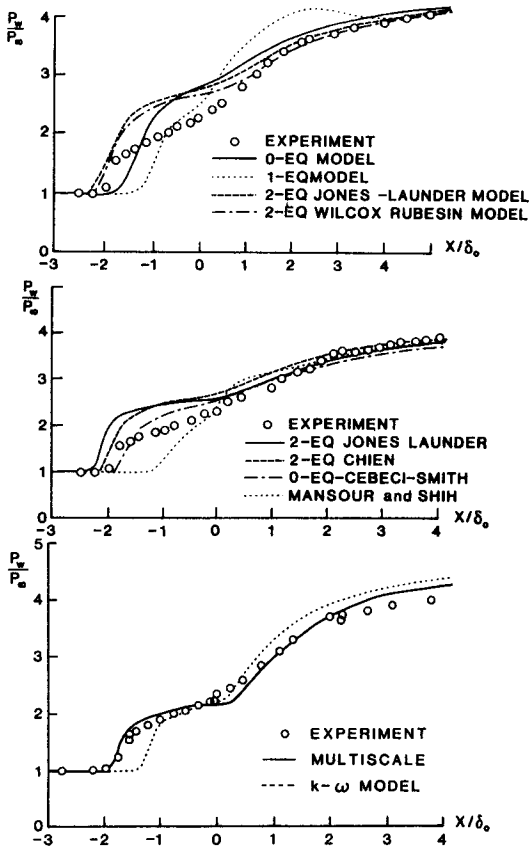


Figure 5.8: Comparison of computed and measured surface pressure for Mach 3 flow into a 24° compression corner for several turbulence models. [From Marshall and Dolling (1992) — Copyright © AIAA 1992 — Used with permission.]

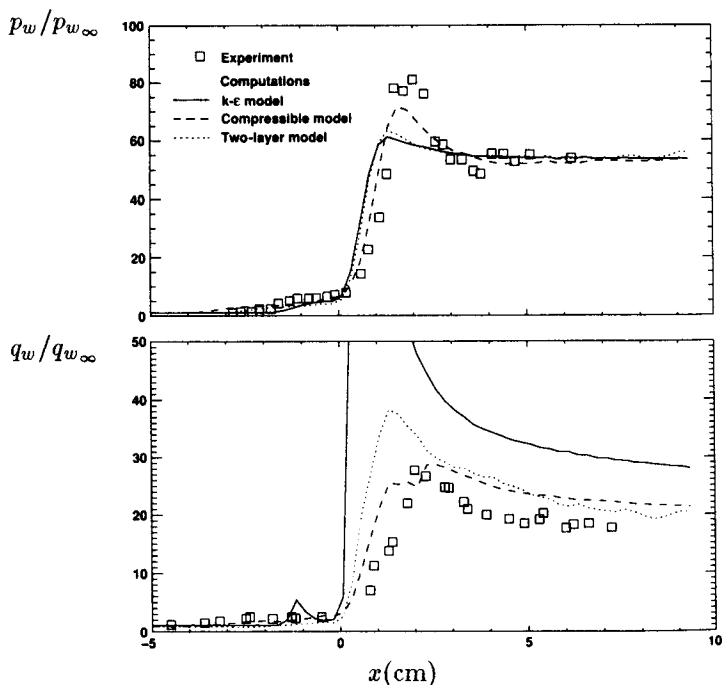


Figure 5.9: Comparison of computed and measured surface pressure and heat transfer for Mach 9.2 flow past a 40° cylinder flare. [From Horstman (1992) — Copyright © AIAA 1992 — Used with permission.]

There has been substantial progress in the capability for prediction of three-dimensional shock wave, turbulent boundary layer interactions. A recent review by Knight (1993) describes the status of research for five basic geometries. Figure 5.10(a) illustrates the three-dimensional single fin, arguably the most extensively studied such interaction. The deflection of the fin surface by an angle α generates an oblique shock that interacts with the boundary layer on the flat plate. This interaction is of some practical interest, as it represents a geometric abstraction of a fin-body juncture for a high-speed aircraft. Figure 5.10(b) compares computed and measured surface pressure for $M_\infty = 2.9$, $\alpha = 20^\circ$, and $Re_{\delta_\infty} = 9 \cdot 10^5$, where δ_∞ is boundary-layer thickness upstream of the interaction. The comparison has been made at a spanwise distance, $z = 6.8\delta_\infty$ from the plane of symmetry. Computations using the Baldwin-Lomax (1978) model (labeled “Knight”) and Rodi’s (1991) $k-\epsilon$ model (labeled “Horstman”) are in close agreement with measurements. Similar close agreement has been obtained with exper-

imental data for pitot pressure and yaw angle [Knight, et al. (1987)]. These results imply that the flowfield is predominantly rotational and inviscid, except within a thin region adjacent to the solid boundaries. This result is similar to the triple-deck theory developed for interacting boundary layers [e.g., Stewartson (1981)] and extended to non-separated three-dimensional shock wave, turbulent boundary layer interactions by Inger (1986). Consequently, the choice of turbulence model is unimportant for comparison with all but the inner (lower deck) provided the upstream boundary layer is correct. However, predicted skin friction and surface heat transfer are very sensitive to the turbulence model chosen, and can exhibit significant disagreement with experiment [Knight (1993)].

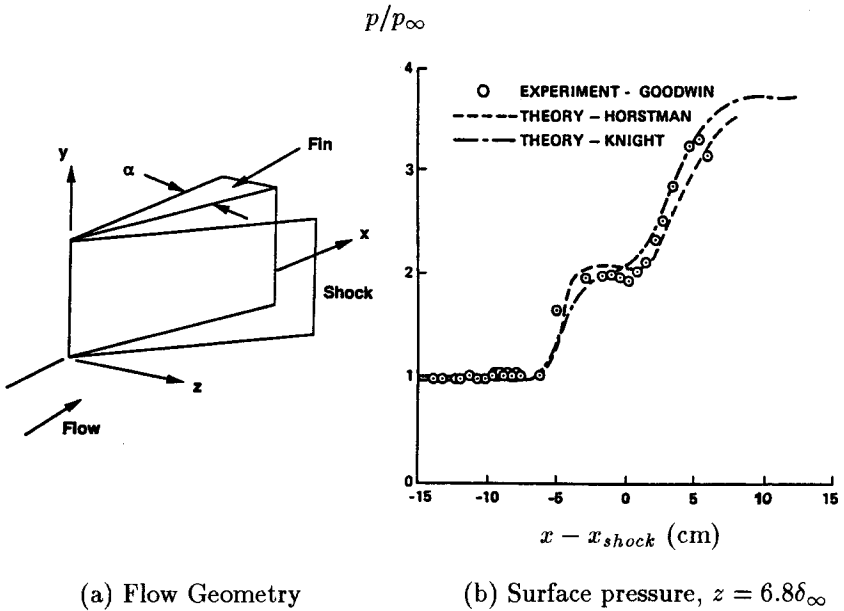
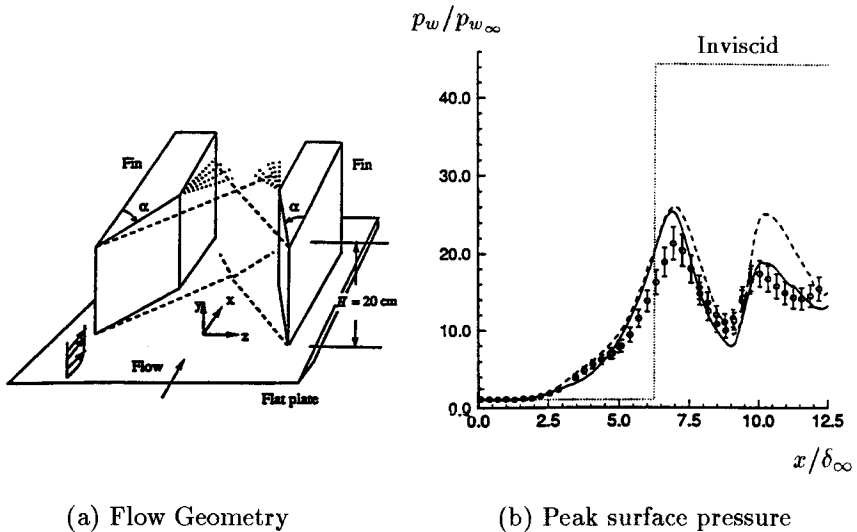


Figure 5.10: Single-fin shock wave, boundary layer interaction; Mach 2.9. [Figure provided by D. D. Knight.]

Figure 5.11(a) shows the double-fin geometry. This geometry is of practical interest as it represents a geometric simplification of a hypersonic inlet using sidewall compression, or a sidewall interaction for a supersonic mixed compression inlet. The two fins generate opposing shocks that intersect on the centerline, and interact with the boundary layers on the flat plate and fin. Figure 5.11(b) compares computed [Narayanswami, Horstman and

Knight (1993)] and measured peak surface pressure (on the centerline) for $M_\infty = 8.3$, $\alpha = 15^\circ$, and $Re_{\delta_\infty} = 1.7 \cdot 10^5$. The turbulence models are the Baldwin-Lomax (1978) model and the Rodi (1991) version of the $k-\epsilon$ model. The predictions are reasonably close except at the peak near $x/\delta_\infty = 10$. Baldwin-Lomax predictions are within about 20% of measurements, while $k-\epsilon$ predictions differ by as much as 45%. It is interesting to note that the peak pressure is approximately half the theoretical inviscid level because of the viscous-inviscid interaction. Reasonable agreement is obtained between computed and measured pitot pressure and yaw-angle profiles. Comparison of computed eddy viscosity shows significant differences, however. As a result, Knight concludes that, similar to the single-fin case, the flow is dominantly rotational and inviscid, except within a thin region near the surface. The turbulence model has a very significant effect on computed heat transfer, and neither model yields acceptable results (Figure 5.12). Although the $k-\omega$ model has not been applied to these flows, we can reasonably conclude that further research is needed in the development and application of turbulence models for three-dimensional shock wave, turbulent boundary layer interactions.



(a) Flow Geometry

(b) Peak surface pressure

Figure 5.11: Double-fin shock wave, boundary layer interaction; Mach 8.3. ● Experiment; — Baldwin-Lomax; - - - Rodi; [Figure provided by D. D. Knight.]

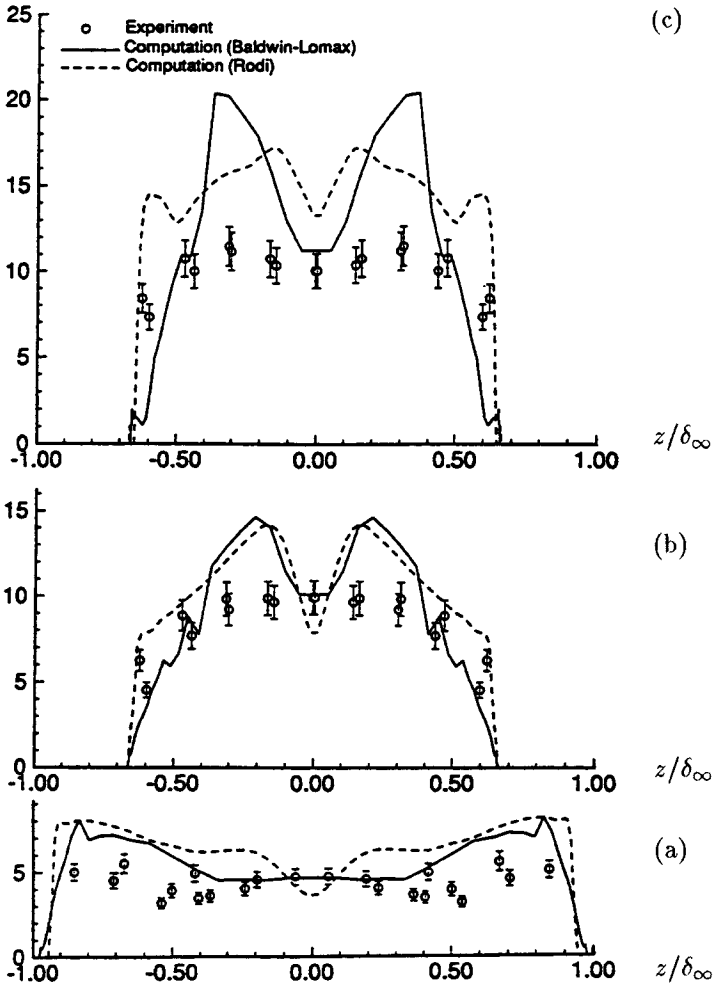
$q_w/q_{w\infty}$ 

Figure 5.12: Transverse profiles of flat plate surface heat transfer at streamwise locations of (a) $x/\delta_\infty = 5.08$, (b) 6.40 and (c) 7.78 for a double-fin shock wave, boundary layer interaction; Mach 8.3. [Figure provided by D. D. Knight.]

Problems

5.1 Derive the Reynolds-averaged momentum-conservation equation for compressible flow.

5.2 Derive the Favre-averaged Reynolds-stress equation [Equation (5.39)].

5.3 Verify that Equations (5.54) and (5.55) are equivalent.

5.4 The classical Crocco temperature-velocity relationship for an adiabatic-wall boundary layer is

$$\frac{T}{T_w} = 1 - A^2 \left(\frac{\tilde{u}}{U_\infty} \right)^2$$

where A is a constant. Use this approximation to evaluate the following integral.

$$u^* = \int_0^{\tilde{u}} \sqrt{\frac{\rho}{\rho_w}} du$$

Compare your result with Equation (5.108).

5.5 To use the WKB method in solving an equation such as

$$\frac{d^2 \omega}{dv^2} - \lambda^2 f(v) \omega = 0, \quad \lambda \rightarrow \infty$$

we assume a solution of the form

$$\omega(v) \sim \exp \left[\lambda \sum_{n=0}^{\infty} S_n(v) \lambda^{-n} \right] \sim \exp [\lambda S_0(v) + S_1(v) + O(\lambda^{-1})]$$

(a) Verify that $S_0(v)$ and $S_1(v)$ are given by

$$S_0(v) = \pm \int \sqrt{f(v)} dv + \text{constant}$$

$$S_1(v) = \ell n |f(v)|^{-1/4} + \text{constant}$$

(b) Use the result of Part (a) to show that the leading-order solution to Equation (5.87) is given by Equations (5.89) and (5.90).

(c) Now, complete the derivation of Equation (5.92).

5.6 Derive the compressible law of the wall implied by the Cebeci-Smith model.

5.7 Using the compressible log-layer solution, show that the turbulence length scale for the k - ω model defined by $\ell = k^{1/2}/\omega$ varies linearly with distance from the surface in the compressible log layer.

5.8 Using the compressible log-layer solution, show that the turbulence length scale for the k - ϵ model defined by $\ell = k^{3/2}/\epsilon$ varies linearly with distance from the surface in the compressible log layer.